

# Embracing Self-Powered Wearables for Intelligent Healthcare Data Management

Wei Gong, *Senior member, IEEE*, Zhaoyuan Xu, *Student member, IEEE*, Longzhi Yuan, *Student member, IEEE*, Haoquan Zhou, Si Chen, *Student member, IEEE*, Yuan Ding, *Member, IEEE*, Amiya Nayak, *Senior member, IEEE*, Jiangchuan Liu, *Fellow, IEEE*

**Abstract**—Existing IoT systems suffer from restricted communication distances, high deployment costs, and frequent battery replacements, making them ineffective for managing healthcare data. This paper presents Prometheus, a self-powered wristband for reporting personal health status over long distances and intelligently managing healthcare data. Prometheus backscatters ambient BLE and ZigBee signals for low-power communication while incorporating a multi-source energy harvester to convert ambient RF, light, and heat into electricity. It also features a biochemical sensor array for monitoring sweat biochemical markers. Prototyped on a flexible PCB, Prometheus demonstrates impressive efficiency, consuming only 5.8 mW for sweat sensing, with BLE and ZigBee transmission energies significantly lower than standard electrochemical workstations and commercial alternatives. Our experiments show consistent signal quality at distances up to 20 meters. In summary, Prometheus emerges as a convenient, efficient, and self-powered wristband, promising to provide ubiquitous healthcare data management in our lives.

**Index Terms**—IoT, ZigBee, BLE, backscatter, data management, sensor, healthcare

## I. INTRODUCTION

Sweat is an easily accessible biofluid that contains a wealth of physiological indicators [1], [2]: abnormal sweat concentrations of  $K^+$  and  $Na^+$  indicate hypokalemia/hyperkalemia and hyponatremia/hypernatremia; sweat chloride level can be used

This work was supported by Natural Science Foundation of China under Grant 62276244, and Research Funds of Centre for Leading Medicine and Advanced Technologies of IHM under Grant 2023IHM01080, 2023IHM01081, 2023IHM01085, and Anhui Provincial Key Research and Development Program under Grant 2022j1102003. We also thank the Information Science Laboratory Center of USTC for the hardware and software services.

An earlier version of this paper was presented at the 19th PerCom 2021 Conferences and was published in its Proceedings. DOI: 10.1109/PERCOM50583.2021.9439117

Corresponding authors: Longzhi Yuan, Haoquan Zhou

Wei Gong and Haoquan Zhou are with the First Affiliated Hospital of USTC, Division of Life Sciences and Medicine, University of Science and Technology of China, Hefei, Anhui, 230001, China (e-mail: weigong@ustc.edu.cn; zhouchq2005@qq.com)

Zhaoyuan Xu and Longzhi Yuan are with the School of Computer Science and Technology at University of Science and Technology of China, Hefei, Anhui, 230001, China (email: xzyjyx@mail.ustc.edu.cn; longzhi@mail.ustc.edu.cn).

Si Chen and Jiangchuan Liu are with the School of Computing Science, Simon Fraser University, Burnaby BC V5A 1S6, Canada (email: sca228@sfsu.ca; jcqliu@sfsu.ca).

Yuan Ding is with the Institute of Sensors, Signals and Systems (ISSS), Heriot-Watt University, Edinburgh, UK (email: yuan.ding@hw.ac.uk).

Amiya Nayak is with the School of Electrical Engineering Computer Science University of Ottawa, ON, Canada (email: amiya.nayak@uottawa.ca).

Copyright (c) 2024 IEEE. Personal use of this material is permitted. However, permission to use this material for any other purposes must be obtained from the IEEE by sending a request to [pubs-perm@ieee.org](mailto:pubs-perm@ieee.org).

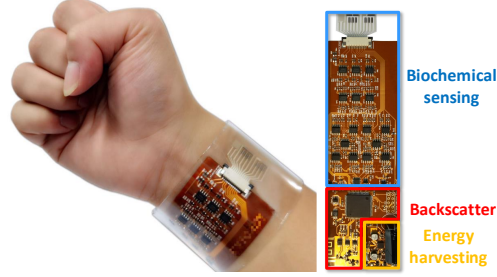


Fig. 1. The self-powered sweat-sensing wristband.

for cystic fibrosis diagnosis; lactic acid in sweat is a sensitive marker for the blood pressure monitor. Effective management of these biochemical indicators in sweat can significantly enhance ubiquitous healthcare services.

In this paper, we ask the following question: can we design a convenient sweat-sensing system that effectively manages the biochemical indicators to continuously report on our health? A lot of research has been carried out in this field [3]–[6]. For example, FISA [3] created an electrochemical wristband, and the entire system is powered by a rechargeable lithium polymer battery. It is not self-sustainable and requires regular battery replacement. [6] built a temporary tattoo-based biosensor that is powered by 396/397 watch batteries, and it suffers from the same battery life issues. A sweat-sensing RFID chip was introduced in [4]. Even though it is passive, RFID technology requires expensive and bulky readers, and the near-field communication distance is very limited. Current sweat-sensing systems suffer from either restricted communication distances, high deployment costs, or frequent battery replacements.

In recent years, backscatter technology has been favored by researchers for its ultra-low power and low cost [7]–[16]. Instead of using power-hungry components (e.g., power amplifiers, frequency synthesizers) for active signal generation, it modulates data on ambient signals like WiFi, BLE, ZigBee, LTE, and LoRa. This technology achieves communication distances of tens of meters and power consumption in the tens of microwatts range, making it a key enabler for ultra-low-power connectivity [7], [17].

As shown in Fig. 1, we propose Prometheus, a self-powered wristband for reporting and intelligently managing healthcare data over long distances. Prometheus distinguishes itself with three key innovations. Firstly, it harnesses BLE and ZigBee backscatter technology for ultra-low-power communication

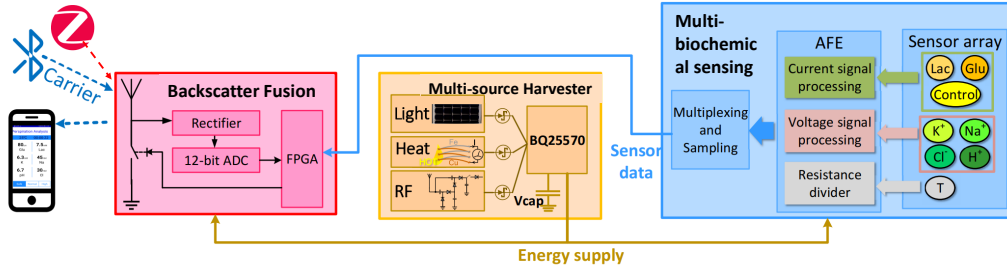


Fig. 2. System overview. Prometheus is composed of three modules for biochemical sensing, energy harvesting and backscatter communication.

with mobile devices and smart appliances, enabling healthcare data transmission over tens of meters. This negates the necessity for dedicated healthcare workstations, utilizing existing IoT devices like smartwatches and tablets as data collectors. Secondly, to ensure sustainability, Prometheus integrates a multi-source energy harvester that converts ambient RF, light, and thermal energy into electricity, enabling uninterrupted monitoring. Lastly, for sweat sensing, Prometheus employs a sensor array to measure various biochemical indicators, providing comprehensive healthcare insights. Worn on the wrist, Prometheus autonomously collects and analyzes sweat data using ambient energy, eliminating the need for hospital visits or expensive monitoring devices, thus enhancing the accessibility of IoT in healthcare management.

We build a prototype of Prometheus with commercial components and conduct extensive experiments to validate its effectiveness. The error rate of glucose concentration is measured within 5%. The biochemical sensing and processing circuit consumes only about 5.8 mW. The backscatter module realizes 180 pJ/bit for BLE transmission and 720 pJ/bit for ZigBee transmission. In conclusion, Prometheus combines biochemical techniques, backscatter technology, and energy harvesting to demonstrate the feasibility of a self-powered biochemical sensing wristband.

## II. SYSTEM OVERVIEW

Fig. 2 presents the Prometheus overview, comprising three modules: backscatter communication, energy harvesting, and biochemical sensing. The backscatter module manages excitation packet identification, RF-switch control, and sensor data transmission. The energy harvesting module harvests energy from ambient RF, light, and heat. The energy convertors, including the solar panel for light, the thermoelectric generator (TEG) for heat, and the rectifier for RF, are not shown in real pictures. The biochemical sensing module, including the biochemical sensor array, processing paths, multiplexer, and ADC, measures the concentrations of sweat biochemical markers. The energy harvesting module powers both the biochemical sensing and backscatter modules. The biochemical sensing module measures the sweat biochemical markers. The low-power FPGA, initially reconfigured from non-volatile flash, identifies ambient BLE/ZigBee packets. Upon identification, it modulates sensor data by controlling RF-switch toggling. After sensor data transmission, it prompts biochemical data acquisition, repeating the process until stored energy is depleted.

## III. BACKSCATTER COMMUNICATION

In this section, we outline the backscatter module design, covering the generation of excitation carriers, backscatter modulation for BLE and ZigBee, and the identification of ambient signals.

### A. Signal generation

State-of-the-art backscatter systems can be divided into two categories: non-single-tone and single-tone systems. Non-single-tone systems utilize codeword translation for modulation, where the tag translates excitation symbols into other valid symbols from the same codebook, resulting in CRC errors [8]. These systems necessitate redundant coding for reliability, significantly reducing throughput. Conversely, single-tone systems generate backscatter signals, denoted by  $C(t)$  for the excitation carrier,  $S(t)$  for sensor data, and  $B(t)$  for the backscatter signal.

$$C(t) = A_c e^{j(2\pi f_c t + \phi_c)} \quad S(t) = A_s e^{j(2\pi f_s t + \phi_s)} \quad (1)$$

$$\begin{aligned} B(t) &= C(t)S(t) = A_c e^{j(2\pi f_c t)} A_s e^{j(2\pi f_s t + \phi_s)} \\ &= A_c A_s e^{j(2\pi(f_c + f_s)t + (\phi_c + \phi_s))} \end{aligned}$$

$f_c$  and  $\phi_c$  keep constant during the modulation. We are able to change  $f_s$  and  $\phi_s$  to generate desired signals like BLE and ZigBee. Backscatter signals are CRC-checked, eliminating the need for redundant coding and requiring only one receiver. In Prometheus, we utilize the single tone from BLE or ZigBee to modulate sensor data.

1) *Single tone generation:* BLE employs frequency modulation, producing a single-frequency tone with a stream of constant '0's and '1's. As shown in Fig. 3(a), a scrambler, utilizing a linear-feedback shift register ( $x^7 + x^4 + 1$ ), ensures randomness in the encoded bitstream, known as data whitening. The register is initialized by the channel number. There is a distinct mapping between the raw bit and the whitened bit, which indicates that reverse engineering can be used to obtain the desired whitened bitstream [7]. ZigBee uses OQPSK for modulation in Fig. 3(b). Every four bits are translated into one of the pseudo-random IQ sequences ( $c_0, c_1, c_2, \dots, c_{30}, c_{31}$ ), known as direct sequence spread spectrum (DSSS) [18]. Specifically, even-indexed chips  $c_0, c_2, c_4, \dots$  represent in-phase components (I), while odd-indexed chips  $c_1, c_3, c_5, \dots$  represent quadrature components (Q). A time offset ( $T_c$ ) in branch Q prevents simultaneous changes in

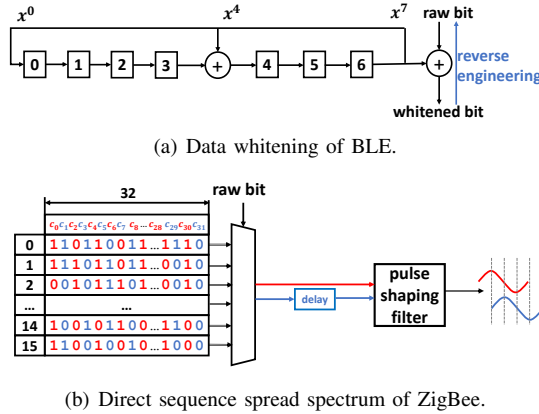


Fig. 3. Generation of BLE and ZigBee signals.

both branches. The I/Q branch then undergoes pulse-shaping filtering, which applies a specific waveform to reduce spectral leakage, as shown in Eq. 2. The combination of branches constructs the ZigBee baseband signal in Eq. 3.  $m$  represents the state of I/Q branches at the edge of consecutive chips.  $f_i$  denotes the signal frequency, and  $\phi_i$  refers to its phase. Previous works [19] [20] have demonstrated continuous phase change at the edge of consecutive chip units, represented by  $\phi_i = \sum_{k=0}^{i-1} (2\pi f_k T_c + \phi_k)$ . With each new chip unit, the only variable left in (3) is  $f_i$ , equivalent to minimum shift keying. While the data flow maps one chip to one frequency shift, the pseudo-random sequence generated by DSSS complicates direct control of the chip stream. While the data flow maps one chip to one frequency shift, the pseudo-random sequence generated by DSSS complicates direct control of the chip stream. Therefore, we can get the ZigBee single-frequency signal by filling the data fields with a constant ‘0’ or ‘1’.

$$p(t) = \begin{cases} \sin(\pi \frac{t}{2T_c}), & \text{input} = 1 \\ -\sin(\pi \frac{t}{2T_c}), & \text{input} = 0 \end{cases} \quad (2)$$

$$\begin{aligned} I(t) + jQ(t) &= \pm \sin(\pi \frac{t}{2T_c} + \frac{m\pi}{2}) \pm j * \sin(\pi \frac{t - T_c}{2T_c} + \frac{m\pi}{2}) \\ &= e^{j(2\pi f_i t + \phi_i)}, m \in \{0, 1\}, k \in \{0, 1, 2, 3\} \end{aligned} \quad (3)$$

2) *Modulation:* We leverage phase shift to modulate BLE/ZigBee. The IPS modulation in IBLE [21] is adopted to modulate BLE. The BLE receiver takes a quadrature demodulator for signal demodulation, which inspires IBLE backscatter signals with different phases. For bit ‘1’ modulation, a square wave at phase  $(\phi_0 + \frac{\pi}{2})$  controls the RF switch, where  $\phi_0$  denotes the phase of the previous square wave. For bit ‘0’, a square wave at phase  $(\phi_0 - \frac{\pi}{2})$  controls the RF switch. A similar strategy is employed for ZigBee modulation, with the difference lying in modulation intervals: BLE modulates every 1 us, while ZigBee modulates every 0.5 us.

### B. Packet identification

Prometheus employs a high-bandwidth rectifier, inspired by RFID and WISP, to directly extract baseband envelopes for identifying excitation signals like BLE and ZigBee with

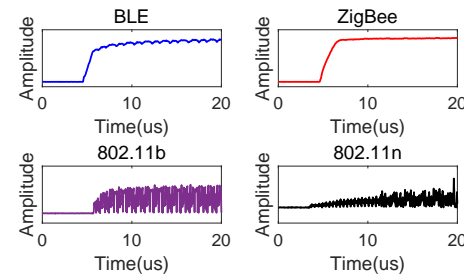


Fig. 4. The extracted baseband signals.

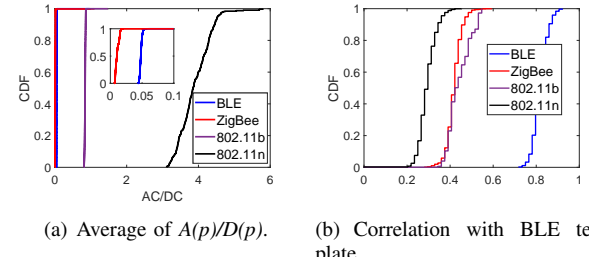


Fig. 5. Signal identification.

ultra-low power [22]. Distinct envelopes for different ambient signals are observed in Fig. 4. To distinguish these signals, we calculate the ratio of AC to DC components:  $D(p) = \frac{\sum_{i=0}^{w-1} V_{base}(p-i)}{w}$ , where  $V_{base}(p)$  is the sampled envelope data,  $D(p)$  is the DC value at time instant  $p$  and  $w$  are the sliding window sizes. The AC component is calculated as:  $A(p) = V_{base}(p) - D(p)$ . The ratio  $AC/DC$  is computed accordingly. The analysis in Fig. 5(a) reveals that for ZigBee, 99.8% of data falls below 0.02, while for BLE, over 99.8% lies between 0.03 and 0.05. Additionally, signals from 802.11b and 802.11n exhibit  $AC/DC$  ratios exceeding 0.8, demonstrating the efficacy of this ratio in identifying BLE/ZigBee from other ambient in-band signals. Given the close distributions of  $AC/DC$  for BLE and ZigBee, we leverage envelope characteristics to distinguish between the two signals. Notably, the distinctive envelope of BLE facilitates signal identification. We cross-correlate the envelope of a pre-stored BLE sequence  $S(p)$  with the excitation signal  $A(p)$ , excluding the DC component  $D(p)$  due to its minimal contribution to packet identification. The signs of  $A(p)$  and  $S(p)$  are used to reduce the computation complexity in the calculation of cross-correlation in Eq. 4. The low-power FPGA AGLN250V2-VQ100I efficiently performs cross-correlation calculations. Fig. 5(b) displays the  $R(i)$  results of 2000 packets, with a sampling rate of 20 MS/s and a template length of 128 samples, indicating consistent cross-correlation values above 0.7 for BLE signals.

$$\begin{aligned} R(i) &= \frac{\sum_{p=1}^L sign(A(p-i))sign(S(p))}{\sqrt{\sum_{p=1}^L |sign(A(p))|} \sqrt{\sum_{p=1}^L |sign(S(p))|}} \\ &= \frac{\sum_{p=1}^L sign(A(p-i))sign(S(p))}{L} \end{aligned} \quad (4)$$

In conclusion, we merge the  $AC/DC$  ratio and cross-correlation for signal identification. BLE is identified if the

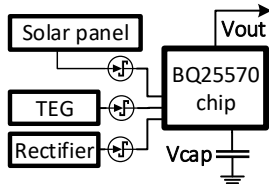


Fig. 6. Harvesting management.

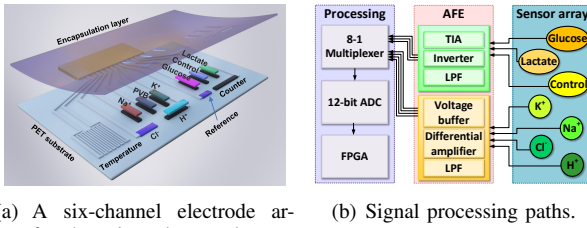


Fig. 7. Biochemical sensing structure.

*AC/DC* ratio is below 0.8 and the correlation result is above 0.7, while ZigBee is identified if the *AC/DC* ratio is below 0.8 and the correlation result is below 0.7.

#### IV. POWER MANAGEMENT

RF, light, and thermal energy are selected as energy sources for their widespread availability [23], [24]. Indoors, WiFi signals offer 0.08 to 1  $\mu\text{W}$  of power, ensuring reliable energy regardless of environmental conditions. The light energy, both indoors and outdoors, ranges from 0.1 to 100  $\text{mW}/\text{cm}^2$ , providing a dependable energy source. Additionally, thermal energy from human skin, reaching 20  $\text{mW}/\text{cm}^2$ , serves as another abundant energy resource due to the wristband's proximity to the body. This diverse range of energy sources enhances the system's universality and sustainability. We use solar panels, thermoelectric generators (TEGs), and rectifier circuits to harvest energy from light, thermal, and RF signals, respectively. The resistance of the TEG at 10°C, the solar panel with 500 Lux light, and the rectifier with 0 dBm RF signal are  $6.12\Omega$ ,  $119K\Omega$ , and  $1.09M\Omega$ , respectively. If those harvesting modules are directly connected to the power management chip (the TI BQ25570 harvesting management chip in the Prometheus system), the TEG, whose resistor is much smaller than the other components, will act as a load and consume a large portion of energy. To prevent energy loss, we isolate each harvesting module using low-dropout Schottky diodes, as depicted in Fig. 6. This ensures that most of the energy is efficiently harvested by the TI BQ25570 power management chip, as the diodes prevent the TEG from acting as a load.

#### V. ENERGY-EFFICIENT SWEAT SENSING

This section describes the sweat-sensing module. Specifically, Prometheus uses a customized biochemical sensor array and signal processing circuits for sweat sensing. The sensor array and the structure of signal processing circuits are shown in Fig. 7.

#### A. Fabrication of biochemical sensor array

Fig. 7(a) illustrates a six-channel electrode array for detecting glucose, lactate,  $\text{Na}^+$ ,  $\text{K}^+$ ,  $\text{H}^+$ , and  $\text{Cl}^-$  in sweat. These electrodes convert the corresponding component concentrations into electrical signals. The amperometric glucose and lactate sensors are based on a traditional three-electrode system integrated with a differential electrode. The glucose oxidase, lactate oxidase, and BSA are modified on three working electrodes, respectively. A carbon electrode serves as the counter electrode, and an  $\text{Ag}/\text{AgCl}$  electrode acts as the reference electrode. The BSA-covered working electrode is employed here as a control electrode to counteract drift and interference. Measurement of  $\text{Na}^+$ ,  $\text{K}^+$ ,  $\text{H}^+$ , and  $\text{Cl}^-$  levels utilizes ion-selective electrodes paired with a PVB-coated reference electrode.

#### B. Differential mode technique for baseline drift

In electrochemical systems, baseline drift can occur due to environmental factors, human movement, or instrument artifacts, making it challenging to accurately measure target molecule concentrations in sweat over time. Various approaches, including the dual-reported method [25], filter technique [26], and compensation algorithm [27] have been proposed to overcome this issue, whereas the mechanism of baseline drift remains unclear. In Prometheus, a differential-measurement method is employed to counteract baseline drift and noise. The schematic of the differential-mode glucose sensor is shown in Fig. 8(a). The electrode array comprises a sensing electrode covered with glucose oxidase (GOx) and a control electrode covered with bovine serum albumin (BSA). BSA is chosen as the control due to its inert nature and stability. Both electrodes respond to environmental effects and biomolecule interference, but only the GOx-covered electrode reacts to glucose. As shown in the block diagram of the differential-mode glucose sensor shown in Fig. 8(b), both the GOx-covered working electrode and the BSA-covered electrode respond to baseband drift caused by environmental effects ( $I_1$ ), noise caused by diverse biomolecules ranging from small electrolytes, and metabolites to hormones and larger proteins in human sweat ( $I_3$ ). But only the GOx-covered electrode responds to the target glucose ( $I_2$ ). The resulting interference and drift signals are counteracted through signal processing and kinetic differential measurement, providing an effective solution for drift correction and interference compensation.

#### C. Signal processing circuit

In the biochemical processing circuitry (Fig. 7(b)), analog circuits are intricately designed to ensure precise resolution of each electrode's output within the ADC's input voltage range. Reverse currents from the glucose and lactate electrodes are measured at the  $\text{Ag}/\text{AgCl}$  electrode, necessitating the use of a trans-impedance amplifier (TIA) to convert current to voltage. As TIA outputs negative voltage for reverse currents, an inverter stage follows to convert them to positive voltages accepted by the ADC. Each path also includes a unity-gain

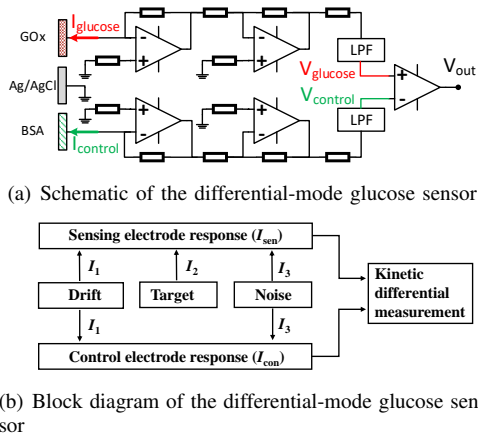


Fig. 8. Biochemical sensor array structure.

low pass filter (LPF) to minimize noise and interference, with a -3 dB frequency at 1 Hz. In the measurement paths for  $H^+$ ,  $Cl^-$ ,  $K^+$ , and  $Na^+$ , the generated signals are the voltage differences between their corresponding ion-selective electrodes (ISE) and PVB-coated shared reference electrode. We directly measure such voltage differences. Every one of their signal processing paths starts with two voltage buffers for the sensor electrode and PVB-coated reference electrode, followed by a differential amplifier and ADC. For the purpose of suppressing noise and interference, the last stage is a low-pass filter.

## VI. IMPLEMENTATION

In this section, we demonstrate the implementation of the three modules for backscatter communication, energy harvesting, and biochemical sensing. Details regarding the power consumption are shown in Appendix A.

### A. Packet identification and backscatter communication

A high-bandwidth rectifier, composed of HSMS-286C, capacitors, and resistors, captures a fine-grained baseband envelope. The rectifier output is sampled by a low-power ADC LTC2366CTS8. Packet identification and RF-switch control are managed by a Microsemi IGLOO nano AGLN250V2-VQ100I FPGA. Excitation signals, including WiFi (802.11b/n), BLE, and ZigBee, are transmitted using laptops with AR938X wireless network adapters, TI CC2640 BLE modules, and CC2530 ZigBee modules.

### B. Energy harvesting

The Prometheus prototype features a 2-layer wristband-shaped flexible PCB measuring 145mm x 45mm. Energy harvesting components include a solar cell MP3-37 (114mm x 37mm) for light energy, six thermoelectric generators TG12-8-01LS connected in series (40mm x 40mm) for heat energy, and a 5-stage voltage doubler circuit using capacitors and HSMS-286C Schottky diodes for RF energy. Power management is handled by the TI energy harvesting chip BQ25570, with a 1000 uF capacitor utilized for energy storage.

### C. Sweat sensing

The signal processing circuitry employs operational amplifiers LT1462ACS8, along with capacitors and resistors. These amplifiers require dual-rail power supplies of +5V and -5V. The booster converter TPS61220 and charge pump voltage inverter TPS60400 are utilized to convert the BQ25570's 3.3V to +5V and -5V, respectively. Processed signals representing glucose, lactate,  $K^+$ ,  $Na^+$ ,  $H^+$ , and  $Cl^-$  levels are directed to an ADC AD7466 through the multiplexer ADG758.

## VII. EVALUATION

In this section, we evaluate the performance of backscatter communication, sweat sensing and analysis, energy harvesting, real-time sensor reading, and data transmission. The efficiency of energy harvesting is shown in Appendix B.

### A. Backscatter communication

**1) Packet identification:** We evaluate BLE/ZigBee packet identification accuracy across varying sampling rates. Two comparison methods are employed: the first utilizes  $AC/DC$  to discern excitation packets, identifying BLE if  $Th_1 < AC/DC < Th_2$  and ZigBee if  $AC/DC < Th_1$ . The second method combines  $AC/DC$  with cross-correlation, identifying BLE if  $R > Th_3$  and  $AC/DC < Th_2$ , and ZigBee if  $R < Th_3$  and  $AC/DC < Th_2$ . Fig. 9(a) and Fig. 9(b) present the experiment results. Both BLE identification methods achieve over 90% accuracy at sampling rates exceeding 2.5 MS/s. However, using only  $AC/DC$  drops below 30% accuracy at 1.25 MS/s, while the alternative algorithm maintains over 75% accuracy. For ZigBee identification,  $AC/DC$  accuracy significantly declines below 30% at 5 MS/s and further drops below 30% at 2.5 MS/s, whereas the alternative algorithm maintains over 85% accuracy at 2.5 MS/s. In terms of identification accuracy with interference, we use a laptop equipped with a Qualcomm Atheros AR938X NIC to transmit 802.11n packets, serving as an interference source. Packet payload size is set to 500 bytes, with transmission rates of 0 pkts/s (no interference), 300 pkts/s (low interference), and 1000 pkts/s (high interference). BLE identification accuracy at a sampling rate of 1.25 Msps is 0.98, 0.84, and 0.47, while ZigBee identification accuracy is 0.95, 0.8, and 0.45, as illustrated in Fig. 9(c). Ambient Wi-Fi transmission introduces interference affecting packet identification.

**2) Throughput, BER, and RSSI:** The throughput, bit error rate (BER), and RSSI are assessed in a hallway setting, with the backscatter sensor positioned 0.2 m from the transmitter and transmission power boosted to about 20 dBm using a power amplifier. Results are depicted in Fig. 9(d), Fig. 9(e), and Fig. 9(f). Fig. 9(d) illustrates Prometheus' BER with increasing uplink range: BLE maintains below 1% BER over 28 m, while ZigBee stays below 1% up to 20 m. Throughput evaluation reveals BLE sustaining over 990 kbps over 28 m, whereas ZigBee throughput decreases to 232 kbps at 20 m. As expected, signal strength for both BLE and ZigBee diminishes with distance.

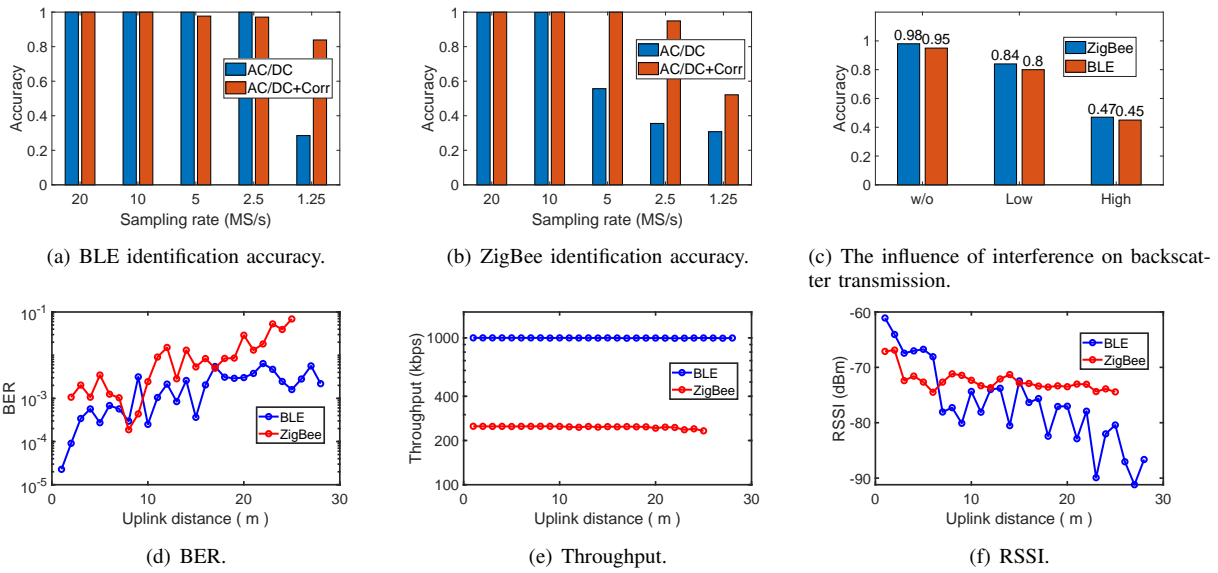
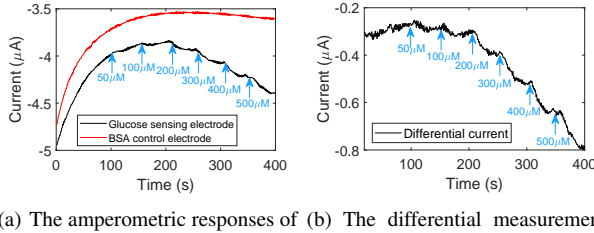


Fig. 9. Identification accuracy and performance of backscatter communication.

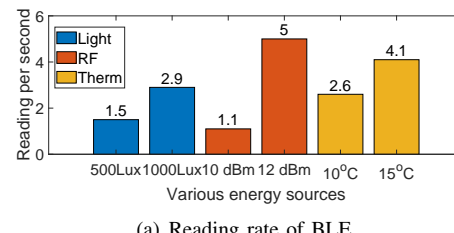


(a) The amperometric responses of the glucose sensing electrode and between the glucose sensing electrode and BSA control electrode to the different concentration of glucose in artificial sweat solution.

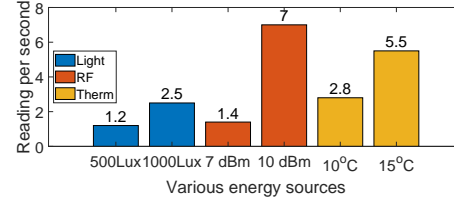
Fig. 10. Differential mode technique.

### B. Sweat sensing and analyzing

Fig. 10 illustrates the successful application of the differential mode technique for glucose monitoring in artificial sweat. The artificial sweat matrix, simulating real sweat samples, includes various components such as pyruvic acid, urea,  $\text{NH}_4\text{Cl}$ ,  $\text{KCl}$ , uric acid, and  $\text{MgCl}_2$ , along with glucose at different concentrations. Fig. 10(a) displays the amperometric responses of a glucose-sensing electrode and a BSA control electrode to glucose solutions spanning a representative sweat concentration range of 0 to 500  $\mu\text{M}$ . The glucose-sensing electrode initially exhibits instability until the glucose concentration reaches 200  $\mu\text{M}$ . Despite an apparent response to 50  $\mu\text{M}$  of glucose, it is obscured by baseline fluctuations. Both the glucose-sensing and BSA control electrodes are affected by baseline drift and interference noise, albeit to a similar extent. However, after differential measurement, interference noise and baseline drift are mitigated, as demonstrated in Fig. 10(b), where differential signals distinctly respond to glucose at a low concentration of 50  $\mu\text{M}$ . Further details on Prometheus's performance in varying temperature environments are provided in Appendix C.



(a) Reading rate of BLE.



(b) Reading rate of ZigBee.

Fig. 11. System reading rate.

### C. Real-time sensor reading and data transmitting

Sensor readings for the glucose electrode, control electrode, lactate electrode,  $K^+$  electrode,  $Na^+$  electrode,  $H^+$  electrode,  $Cl^-$  electrode, and the temperature are transmitted. For each reading, only 8 bits of a 12-bit ADC output are transmitted and analyzed. Therefore, there are in total  $8 \times 8 = 64$  bits for transmission. We perform reverse engineering for BLE advertising packets, whose single tone lasts for 248  $\mu\text{s}$ . Theoretically, it can generate BLE packets with a payload length of 16 bytes. Similarly, ZigBee packets, comprising a single tone lasting 508  $\mu\text{s}$ , can be created with an 8-byte data field by reducing the preamble field to 28 bits.

Fig. 11 shows that with 500 Lux office light, our system can receive and decode 1.5 BLE and 1.2 ZigBee packets per second. At 1000 Lux, this increases to 2.9 BLE and 2.5 ZigBee packets. Using RF energy or human heat, BLE readings can reach 5 and 4.1 per second, respectively, while

ZigBee readings can reach 7 and 5.5 per second. Considering that the needed data-refreshing rate of those sensor data can be as low as 1 reading every 5 minutes, our data transmission rate is sufficiently high.

### VIII. DISCUSSION

**Application scenarios:** Prometheus is promising to communicate with BLE/ZigBee health monitoring devices. BLE healthcare monitoring devices include pulse oximeters [28], blood pressure monitors [29], body fat scales [30], etc. Additionally, PIR motion sensors [31], pulse detectors [32], ECG machines [33], etc. communicate with ZigBee signals. Prometheus can upload monitored healthcare indicators to these devices without dedicated workstations or readers.

**Scalability:** The Prometheus prototype supports BLE and ZigBee connectivity, with hardware compatibility for other protocols [7], [8], [17], [34]–[36]. For instance, it can integrate with edge servers to perform BLE backscatter, and emulate a passive BLE protocol stack [37]. Additionally, Prometheus can decode WiFi packets by detecting WiFi signal envelopes, enabling native connectivity via ambient WiFi signals [38]. It can also utilize uncontrolled LTE signals for healthcare data transmission and decode LoRa packets with SAW filters, facilitating health monitoring in outdoor environments [39], [40].

### IX. CONCLUSION

This paper presented Prometheus, the first self-powered sweat-sensing wristband capable of reporting personal health status over long distances and intelligently managing healthcare data. Harvesting multiple ambient energies, it is capable of monitoring human sweat and transmitting sensor data at a range of over 20 m.

### REFERENCES

- [1] M. Bariya, H. Y. Y. Nyein, and A. Javey, "Wearable sweat sensors," *Nature Electronics*, vol. 1, pp. 160–171, 2018.
- [2] A. Koh, D. Kang, Y. Xue, S. Lee, R. M. Pielak, J. Kim, T. Hwang, S. Min, A. Banks, P. Bastien *et al.*, "A soft, wearable microfluidic device for the capture, storage, and colorimetric sensing of sweat," *Science translational medicine*, vol. 8, pp. 366 165–366 165, 2016.
- [3] W. Gao, S. Emaminejad, H. Y. Y. Nyein, S. Challa, K. Chen, A. Peck, H. M. Fahad, H. Ota, H. Shiraki, D. Kiriyama *et al.*, "Fully integrated wearable sensor arrays for multiplexed in situ perspiration analysis," *Nature*, vol. 529, pp. 509–514, 2016.
- [4] D. P. Rose, M. E. Ratterman, D. K. Griffin, L. Hou, N. Kelley-Loughnane, R. R. Naik, J. A. Hagen, I. Papautsky, and J. C. Heikenfeld, "Adhesive rfid sensor patch for monitoring of sweat electrolytes," *IEEE Transactions on Biomedical Engineering*, vol. 62, no. 6, pp. 1457–1465, 2014.
- [5] M. Qiu, W. Dai, and A. V. Vasilakos, "Loop parallelism maximization for multimedia data processing in mobile vehicular clouds," *IEEE Transactions on Cloud Computing*, vol. 7, pp. 250–258, 2016.
- [6] J. Kim, I. Jeerapan, S. Imani, T. N. Cho, A. Bandodkar, S. Cinti, P. P. Mercier, and J. Wang, "Noninvasive alcohol monitoring using a wearable tattoo-based iontophoretic-biosensing system," *Acs Sensors*, vol. 1, no. 8, pp. 1011–1019, 2016.
- [7] V. Iyer, V. Talla, B. Kellogg, S. Gollakota, and J. Smith, "Inter-technology backscatter: Towards internet connectivity for implanted devices," in *Proc. ACM SIGCOMM*, 2016, p. 356–369.
- [8] P. Zhang, C. Josephson, D. Bharadia, and S. Katti, "Freerider: Backscatter communication using commodity radios," in *Proc. ACM CONEXT*, 2017.
- [9] Z. Chi, X. Liu, W. Wang, Y. Yao, and T. Zhu, "Leveraging ambient lte traffic for ubiquitous passive communication," in *Proc. ACM SIGCOMM*, 2020, p. 172–185.
- [10] K. Liu, Q. Ma, W. Gong, X. Miao, and Y. Liu, "Self-diagnosis for detecting system failures in large-scale wireless sensor networks," *IEEE Transactions on Wireless Communications*, vol. 13, no. 10, pp. 5535–5545, 2014.
- [11] W. Wu, X. Wang, A. Hawbani, L. Yuan, and W. Gong, "A survey on ambient backscatter communications: Principles, systems, applications, and challenges," *Computer Networks*, vol. 216, p. 109235, 2022.
- [12] H. Wang and W. Gong, "Rf-pen: Practical real-time rfid tracking in the air," *IEEE Transactions on Mobile Computing*, vol. 20, pp. 3227–3238, 2021.
- [13] W. Gong, I. Stojmenovic, A. Nayak, K. Liu, and H. Liu, "Fast and scalable counterfeits estimation for large-scale rfid systems," *IEEE/ACM Transactions on Networking*, vol. 24, no. 2, pp. 1052–1064, 2016.
- [14] J. Yu, J. Liu, R. Zhang, L. Chen, W. Gong, and S. Zhang, "Multi-seed group labeling in rfid systems," *IEEE Transactions on Mobile Computing*, vol. 19, no. 12, pp. 2850–2862, 2020.
- [15] W. Gong, J. Liu, and Z. Yang, "Fast and reliable unknown tag detection in large-scale rfid systems," in *Proc. ACM MobiHoc*, 2016, p. 141–150.
- [16] J. Zhao, J. Liu, H. Wang, C. Xu, W. Gong, and C. Xu, "Measurement, analysis, and enhancement of multipath tcp energy efficiency for datacenters," *IEEE/ACM Transactions on Networking*, vol. 28, pp. 57–70, 2020.
- [17] Z. Xu and W. Gong, "Bumblebee: Enabling the vision of pervasive zigbee backscatter communication," in *Proc. IEEE PerCom*, 2023, pp. 252–261.
- [18] "Ieee standard for information technology– local and metropolitan area networks– specific requirements– part 15.4: Wireless medium access control (mac) and physical layer (phy) specifications for low rate wireless personal area networks (wpans)," *IEEE Std 802.15.4-2006*, pp. 1–320, 2006.
- [19] <https://www.ti.com/product/CC2420>.
- [20] J. Notor, A. Caviglia, and G. Levy, "Cmos rfic architectures for ieee 802.15. 4 networks," *Cadence Design Systems, Inc*, vol. 41, 2003.
- [21] M. Zhang, S. Chen, J. Zhao, and W. Gong, "Commodity-level ble backscatter," in *Proc. ACM Mobicom*, 2021, p. 402–414.
- [22] M. Philipose, J. Smith, B. Jiang, A. Mamishev, S. Roy, and K. Sundara-Rajan, "Battery-free wireless identification and sensing," *IEEE Pervasive Computing*, vol. 4, pp. 37–45, 2005.
- [23] R. J. Vullers, R. v. Schaijk, H. J. Visser, J. Penders, and C. V. Hoof, "Energy harvesting for autonomous wireless sensor networks," *IEEE Solid-State Circuits Magazine*, vol. 2, pp. 29–38, 2010.
- [24] F. Dehbashi, A. Abedi, T. Brecht, and O. Abari, "Verification: can wifi backscatter replace rfid?" in *Proc. ACM MobiCom*, 2021, p. 97–107.
- [25] H. Li, N. Arroyo-Curras, D. Kang, F. Ricci, and K. W. Plaxco, "Dual-reporter drift correction to enhance the performance of electrochemical aptamer-based sensors in whole blood," *Journal of the American Chemical Society*, vol. 138, pp. 15 809–15 812, 2016.
- [26] T. Roberts, C. Braban, C. Oppenheimer, R. Martin, R. Freshwater, D. Dawson, P. Griffiths, R. Cox, J. Saffell, and R. Jones, "Electrochemical sensing of volcanic gases," *Chemical Geology*, vol. 332, pp. 74–91, 2012.
- [27] D. Chen and P. K. Chan, "An intelligent isfet sensory system with temperature and drift compensation for long-term monitoring," *IEEE Sensors Journal*, vol. 8, pp. 1948–1959, 2008.
- [28] <https://thedigitalhealthstore.com/collections/bluetooth-devices/products/air-wireless-pulse-oximeter-ihealthlabs/>.
- [29] <https://www.dusuniot.com/product-specification/blood-pressure-monitor-spec/>.
- [30] <https://www.medicalnewstoday.com/articles/body-fat-scale#summary>.
- [31] <https://www.dusuniot.com/product/smart-pir-sensor/>.
- [32] <https://www.dusuniot.com/case-study/remote-patient-monitoring-iot\pulse-oximeter-at-taikang-community/>.
- [33] <https://www.dusuniot.com/case-study/remote-patient-monitoring-iot\pulse-oximeter-at-taikang-community/>.
- [34] Q. Wang, S. Chen, J. Zhao, and W. Gong, "Rapidrider: Efficient wifi backscatter with uncontrolled ambient signals," in *Proc. IEEE INFOCOM*, 2021, pp. 1–10.
- [35] Z. Xu and W. Gong, "Enabling zigbee backscatter communication in a crowded spectrum," in *Proc. IEEE ICNP*, 2022, pp. 1–11.
- [36] Z. Xu, Y. Ding, and W. Gong, "A fine-grained modulation technology for zigbee backscatter communication," in *Proc. IEEE MMS*, 2022, pp. 1–4.
- [37] M. Jiang and W. Gong, "Dances with blues: Harnessing multi-frequency carriers for commodity bluetooth backscatter," vol. 1, 2023.

- [38] L. Yuan and W. Gong, "Enabling native wifi connectivity for ambient backscatter," in *Proc. ACM MobiSys*, 2023, p. 423–435.
- [39] Y. Feng, S. Chen, W. Xi, S. Wang, J. Zhao, and W. Gong, "Heartbeating with lte networks for ambient backscatter," in *IEEE Transactions on Mobile Computing*, 2023, pp. 1–12.
- [40] X. Guo, L. Shangguan, Y. He, N. Jing, J. Zhang, H. Jiang, and Y. Liu, "Saiyan: Design and implementation of a low-power demodulator for LoRa backscatter systems," in *Proc. USENIX NSDI*, 2022, pp. 437–451.



**Si Chen** (Student Member, IEEE) received the bachelor's degree from the China University of Geosciences and the master's degree from Simon Fraser University, where she is currently pursuing the Ph.D. degree with the School of Computing Science. Her research interests include wireless networks and big data.



**Wei Gong** (M'14) is a Professor with the School of Computer Science and Technology at University of Science and Technology of China. He received his B.S. degree from the Department of Computer Science and Technology at Huazhong University of Science and Technology, M.S. and Ph.D. degrees in the School of Software and Department of Computer Science and Technology at Tsinghua University. His research interests include backscatter networks, edge system, and IoT applications.



**Yuan Ding** received his Bachelor's degree from Beihang University (BUAA), Beijing, China, in 2004, Master's degree from Tsinghua University, Beijing, China, in 2007, and Ph.D. degree from Queen's University of Belfast, Belfast, UK, in 2014, all in Electronic Engineering. He is now an Assistant Professor at the Institute of Sensors, Signals and Systems (ISSS) in Heriot-Watt University, Edinburgh, UK. His research interests are in IoT-related physical-layer designs, antenna array, physical layer security, and 5G related areas. He was the recipient of the IET Best Student Paper Award at LAPC 2013 and the recipient of the Young Scientists Awards in General Assembly and Scientific Symposium (GASS), 2014 XXXIst URSI.



**Zhaoyuan Xu** received the B.S. degree in computer science and technology from University of Science and Technology of China, Anhui Province, China. He is currently pursuing the M.S. degree with School of Computer Science and Technology, University of Science and Technology of China. His research interests include backscatter communication and IoT application.



**Longzhi Yuan** received his B.S. degree from School of Information Science and Technology, University of Science and Technology of China, Anhui Province, China, in 2017. He is a Ph.D. student in School of Data Science, University of Science and Technology of China, under supervision of Dr. Wei Gong. His research interests include wireless networks and IoT.

**Amiya Nayak** received his B.Math. degree in Computer Science and Combinatorics and Optimization from University of Waterloo, Canada, in 1981, and Ph.D. in Systems and Computer Engineering from Carleton University, Canada, in 1991. He has over 17 years of industrial experience in software engineering, avionics and navigation systems, simulation and system level performance analysis. He has served in the Editorial Board of several journals, including *IEEE Transactions on Parallel and Distributed Systems*, *International Journal of Parallel, Emergent and Distributed Systems*, *Journal of Sensor and Actuator Networks*, and *EURASIP Journal of Wireless Communications and Networking*. Currently, he is a Full Professor at the School of Electrical Engineering and Computer Science at the University of Ottawa. His research interests include mobile computing, software-defined networking, wireless sensor networks, and vehicular ad hoc networks.



**Haoquan Zhou** received both the Bachelor's degree from School of Medicine, Anhui University of Science and Technology, and Master's degree from Bengbu Medical College. His research interests include Wise Information Technology of med.



**Jiangchuan Liu** received the B.Eng. degree (cum laude) in computer science from Tsinghua University, Beijing, China, in 1999, and the Ph.D. degree in computer science from The Hong Kong University of Science and Technology in 2003. He is currently a University Professor with the School of Computing Science, Simon Fraser University, BC, Canada. He is also a NSERC E.W.R. Steacie Memorial Fellow. He was a co-recipient of the Inaugural Test of Time Paper Award of IEEE INFOCOM in 2015, the ACM SIGMM TOMCCAP Nicolas D. Georganas Best Paper Award in 2013, and the ACM Multimedia Best Paper Award in 2012. He has served on the Editorial Boards of *IEEE/ACM TRANSACTIONS ON NETWORKING*, *IEEE TRANSACTIONS ON BIG DATA*, *IEEE TRANSACTIONS ON MULTIMEDIA*, *IEEE COMMUNICATIONS SURVEYS AND TUTORIALS*, and *IEEE INTERNET OF THINGS JOURNAL*. He is also a Steering Committee Member of *IEEE TRANSACTIONS ON MOBILE COMPUTING*.

